

# Different ocular dominance map formation influenced by orientation preference columns in visual cortices

Myoung Won Cho\* and Seunghwan Kim†

*Asia Pacific Center for Theoretical Physics and Nonlinear & Complex Systems Laboratory - NRL,  
Department of Physics, Pohang University of Science and Technology, Pohang, Gyeongbuk, 790-784, Korea*

In animal experiments, the observed orientation preference (OP) and ocular dominance (OD) columns in the visual cortex of the brain show various pattern types. Here, we show that the different visual map formations in various species are due to the crossover behavior in anisotropic systems composed of orientational and scalar components such as easy-plane Heisenberg models. We predict the transition boundary between different pattern types with the anisotropy as a main bifurcation parameter, which is consistent with experimental observations.

PACS numbers: 42.66.-p, 75.10.Hk, 89.75.Fb

The highly ordered structure in the mammalian visual cortex has attracted much attention from theoretical neurobiologists and has been thoroughly studied with the expectation of providing the basis for neural dynamics and computational models. Though most models of the visual map formation are based on common postulates, such as Hebbian synapses, connections or competitions between neighboring neurons and synaptic normalization, there are quite a number of successful models with unique mechanisms [1, 2]. The Hamiltonian models with spin variables were proposed for the visual map formation with a striking analogy with the physical systems, such as magnetism [3, 4]. Recently, the characteristics of visual maps are systematically explored through the statistical properties of vortices in magnetism [5]. The spin-like Hamiltonian models represent essential ingredients of neural interactions in the visual map formation without paying much attention to particular neural control mechanisms and can be shown to exhibit common statistical properties of the vortex formation as in other development models [6].

As vast experimental data on visual maps are accumulated, the various patterns in visual cortices of different animals have drawn much interest with the expectation of testing different neural models experimentally [7, 8, 9, 10, 11, 12, 13]. The observed visual patterns can be classified as at least three different types. In macaque monkeys, the OD columns form parallel bands of regular spacing with relatively few branching points that are mainly oriented perpendicular to area boundaries [7]. The degree of OD segregation is strong and the typical average spacing of OD,  $\Lambda_{OD}$ , is larger than that of the OP columns,  $\Lambda_{OP}$  ( $\Lambda_{OD} > \Lambda_{OP}$ ) [8]. In cats and ferrets, OD columns form an array of beaded bands exhibiting only a weak tendency of elongation perpendicular to area boundaries [9, 10, 11]. The degree of OD segregation is intermediate with  $\Lambda_{OD} < \Lambda_{OP}$  [12]. In the case of tree shrews, the OD segregation is very weak or absent, while more stripe-like patterns are observed in extensive OP columnar regions with low densities of

orientation centers [13].

Some experimental works show that the OP and OD patterns are structurally correlated. The singular points, so-called pinwheels, in OP columns tend to align with the centers of OD bands and the iso-orientation contours intersect the borders of OD bands at right or steep angles [8]. Such correlations between two columns occur due to the normalization of the synapse strength [14]. The average response of the orientation selectivity vanishes at singularities, so that the strong OD components can develop near pinwheels. The orthogonality between contours of the columnar patterns can be explained intuitively through the isotropic Heisenberg model [5]. The different visual pattern types originate from both the synaptic normalization and the anisotropic interaction between two columns. The parameter  $\lambda$ , a measure of the anisotropy between the columns, turns out to be crucial in determining not only the pinwheel stability but also OD pattern types and OP pattern regularity. We estimate the anisotropy for each species from the typical spacing of OP and OD patterns from experiments. We calculate the threshold of anisotropy between different OD pattern types and construct the phase diagram, which are consistent with experimental observations.

One of reasons why so many different neural models lead to the successful formation of visual maps is that the typical characteristics of self-organizing maps are determined by the topology of lattice and feature space rather than the detailed cortical modification rules. The statistical properties of emergent cortical maps can be predicted using only minimal mathematical constraints such as the symmetry. In the fiber bundle map (FBM) representation method, the phases of feature components are described by the continuous group corresponding to the manifold in the feature space [5, 6]. Because OP columns have  $O(2)$  (or  $U(1)$ ) symmetry, the energy functions for the OP map formation should be invariant under gauge transformations and take a general form

$$E_{OP} = \int d\mathbf{r} \left\{ \frac{v}{2} |(\nabla - i\mathbf{A})\psi_{OP}|^2 - \frac{m^2}{2} |\psi_{OP}|^2 + \dots \right\} \quad (1)$$

for the orientational feature components  $\psi_{OP}(\mathbf{r}) = (q(\mathbf{r}) \cos 2\phi(\mathbf{r}), q(\mathbf{r}) \sin 2\phi(\mathbf{r}))$  (or  $q(\mathbf{r})e^{2i\phi(\mathbf{r})}$ ) with the preferred angle  $\phi(\mathbf{r})$  and the degree of preference  $q(\mathbf{r})$  at the cortical location  $\mathbf{r}$ . This can be obtained also from other map formation models after a continuum approximation and can explain most typical properties of OP patterns found in experiments and simulations [5].

Biologically the cortical modules are composed of several layers and the different feature components are found from the selective response properties of corresponding layers. Each layer can have a different synaptic strength, so that the energy for the combined OP and OD map formation takes an anisotropic form

$$E = \int d\mathbf{r} \left\{ \frac{v_{OP}}{2} |(\nabla - i\mathbf{A}_{OP})\psi_{OP}|^2 - \frac{m_{OP}^2}{2} |\psi_{OP}|^2 \right. \quad (2)$$

$$\left. + \frac{v_{OD}}{2} |(\nabla - i\mathbf{A}_{OD})\psi_{OD}|^2 - \frac{m_{OD}^2}{2} |\psi_{OD}|^2 \right\}$$

including the scalar component representation of OD  $\psi_{OD}$ . The restriction imposed by the normalization for the total feature vector  $\psi(\mathbf{r}) = (\psi_{OP}(\mathbf{r}), \psi_{OD}(\mathbf{r}))$  is that

$$|\psi(\mathbf{r})|^2 = |\psi_{OP}(\mathbf{r})|^2 + |\psi_{OD}(\mathbf{r})|^2 = const \quad (3)$$

for all  $\mathbf{r}$ . The normalization and the equilibrium ( $\nabla^2 \psi_\mu \sim 0$  for  $\mu = OP$  and  $OD$ ) conditions lead to the orthogonality between OP and OD contour lines, that is  $\nabla \psi_{OP} \cdot \nabla \psi_{OD} \sim 0$ . Now, we define a parameter  $\lambda = m_{OD}^2/m_{OP}^2$  describing the anisotropy between two columns. Then Eq.(2) has two different solutions depending on the anisotropy  $\lambda$ . If  $\lambda < 1$  (or  $\lambda > 1$ ), it has a ground state at the energy density  $-m_{OP}^2/2$  (or  $-m_{OD}^2/2$ ) with weak OD segregations  $\langle \psi_{OD}^2 \rangle = 0$  (or strong OD segregations  $\langle \psi_{OD}^2 \rangle = |\psi|^2$ ). The previous studies in magnetism have shown that there exists another threshold  $\lambda_c$  when features are composed of orientational and scalar components. The statistical properties of visual maps are closely related to those of the classical two-dimensional anisotropic Heisenberg model (CTDAHM), described by the Hamiltonian

$$H = -J \sum_{\langle ij \rangle} (S_i^x S_j^x + S_i^y S_j^y + \lambda S_i^z S_j^z), \quad (4)$$

for  $J > 0$ . The possibility of two vortex types, named in-plane and out-of-plane, in the CTDAHM was first discussed by Takeno and Homma [15]. Different values of the critical anisotropy  $\lambda_c$ , above which out-of-plane vortices become stable, were found to exist and depend on the lattice type ( $\lambda_c \approx 0.72, 0.82, 0.62$  for square, honeycomb, and triangular lattices, respectively) [16].

In this Letter, the anisotropic Heisenberg model with distance-dependent interactions is used for simulations :

$$H = - \sum_{i,j} \{ D_{OP}(r_{ij})(S_i^x S_j^x + S_i^y S_j^y) + D_{OD}(r_{ij})S_i^z S_j^z \} \quad (5)$$

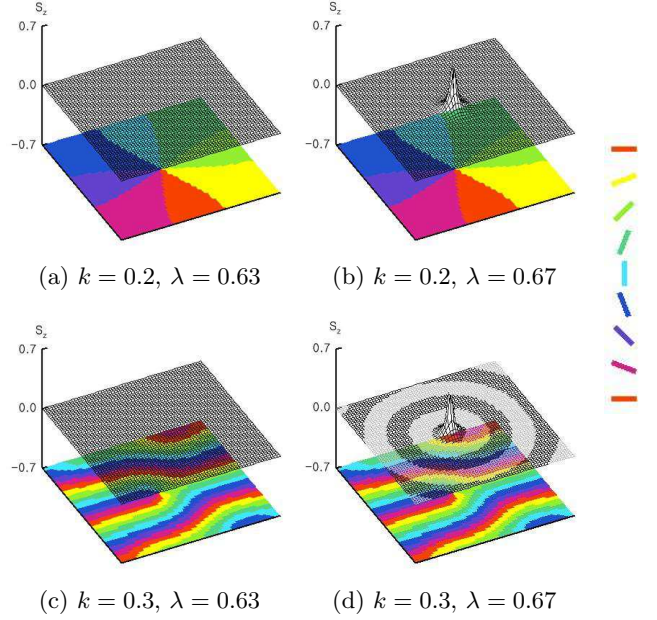


FIG. 1: Development of the scalar peak near the orientational singularity. The preferred angle  $\phi$  is denoted in 8 colors and the ocular dominance  $S_z$  is denoted in black and white wired frames, where the black denotes the region with  $S_z \geq 0$  and the white, otherwise. Simulations are done for the Hamiltonian in Eq.(5) with  $\sigma_{OD}^2 = \sigma_{OP}^2 = 6$ ,  $k_{OD} = k_{OP}$  ( $\lambda = \varepsilon_{OD}/\varepsilon_{OP}$ ). ( $60 \times 60$  lattice and a non-periodic boundary condition)

for the preferred angle  $\phi_i = (1/2) \tan^{-1}(S_i^y/S_i^x)$ , the OD  $S_i^z$  with normalization to a unit modulus ( $|\mathbf{S}_i|^2 = 1$ ). This satisfies also the energy form in Eq.(2) in a continuum approximation. Other development models, such as the elastic-net model or Kohonen's SOFM algorithm, can be rewritten into the spin-like Hamiltonian model [6]. Usually  $D(\mathbf{x}, \mathbf{y}) = D(|\mathbf{x} - \mathbf{y}|)$  is positive in short-range and negative in long-range, that is, of the Mexican hat type. The typical parameters in Eq.(1) or (2) and the exact anisotropy  $\lambda$  are determined by the actual form of  $D(r)$ . In general, the interaction strength within each column is proportional to the activity strength  $\varepsilon_\mu$ , so that  $\lambda \propto \varepsilon_{OD}/\varepsilon_{OP}$ , and to the number of interacting pairs, so that  $\lambda \propto \sigma_{OD}^2/\sigma_{OP}^2$  in two-dimension for the cooperation range  $\sigma_\mu$ . We take the form of the interaction function

$$D_\mu(r) = \varepsilon_\mu \left( 1 - k_\mu \frac{r^2}{\sigma_\mu^2} \right) \exp(-r^2/2\sigma_\mu^2) \quad (6)$$

for an inhibitory strength  $k_\mu$ . Single vortex simulations in Fig. 1 show the structure of two vortex types. When  $\lambda$  is above the threshold  $\lambda_c$ , a peak in the OD map starts to develop near a singular point in the OP map (Fig. 1b and 1d). When there exists a weak inhibitory activity, we have ferromagnetic solutions with both a scalar peak and an orientational singularity (Fig. 1b), which are the typical features of in-plane and out-of-plane vortices ob-

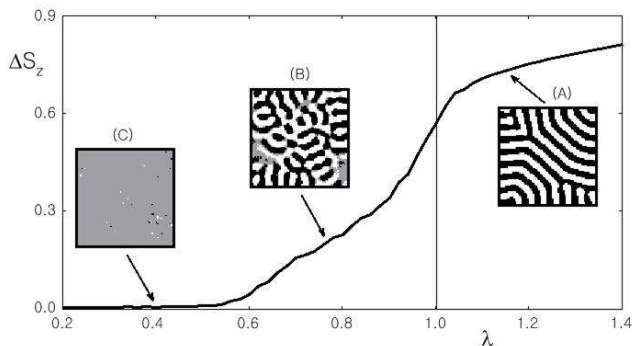


FIG. 2: (a) Different OD pattern formations depending on the anisotropy  $\lambda$ . The gray color in boxes denotes the weak segregation region ( $|S_z| \leq 0.01$ ). Parameters are  $\sigma_{OP}^2 = \sigma_{OD}^2 = 6$ ,  $k_{OP} = k_{OD} = 1.0$  ( $\lambda = \varepsilon_{OD}/\varepsilon_{OP}$ ). Maps are generated using the Metropolis algorithm at zero temperature, with a non-periodic boundary condition and an initially random state in the  $70 \times 70$  lattice.

served in the CTDAHM. Similar results can be obtained in different map formations models, if they are modified to have an anisotropy between columns.

Fig. 2 shows the emergence of three different pattern types in OD columns; Type (A) for  $\lambda > 1$ , parallel bands with strong OD segregation, Type (B) for  $\lambda_c < \lambda < 1$ , beaded bands with intermediate OD segregation, and Type (C) for  $\lambda < \lambda_c$ , the absence of OD segregation. Types (A), (B), and (C) in Fig. 2 correspond to observed OD patterns in macaque monkeys, cats, and tree shrews, respectively. We measure the degree of OD segregation in terms of the standard deviation of  $S_z$  at a given time that is averaged over 10 trial evolutions for a given  $\lambda$ . We find that the OD segregation strength increases as  $\lambda$  increases. The in-plane vortices are unstable under small thermal fluctuations for  $\lambda < 1$ . The anisotropy  $\lambda$  is related to the pinwheel stability and connected to the measured pinwheel density for different animals [5, 17]. Beaded bands are not permanent structure as well and disappear as pinwheels annihilate during the map development process.

For  $\lambda > 1$ , which corresponds to the Ising model region, the OD columns play a dominant role in the overall map formations. Parallel bands appear in a whole range of the OD map and make a right or steep angle with area boundaries, which are the typical properties of OD maps generated without OP columns. In the OP columns, singular points and periodic patterns still exist, but are much less regular. The distribution of iso-orientation contours is not uniform with locally dense or sparse regions (see Fig. 3b). The rotational plane defined from the gradient directions in the feature space helps to understand this point. For  $\lambda = 1$ , the map formation process is balanced between two stationary solutions with the normal vector of the rotational

plane slanted at  $|\hat{n}_x| = |\hat{n}_y| = |\hat{n}_z| = 1/\sqrt{3}$ , so that  $\Delta S_z = \sqrt{1 - |\hat{n}_z|^2}/\sqrt{2} = 1/\sqrt{3} \simeq 0.577$ , as seen in Fig. 2. For  $\lambda > 1$  (or  $\lambda < 1$ ), the rotational plane lies more vertically (or horizontally), so that  $\Delta S_z$  approaches 1 (or 0) as the map formation progresses. If the rotational plane becomes too slanted, the circular trajectories are projected to elongated ellipses in the  $S_x - S_y$  plane, leading to irregularities in  $\phi$  coordinates.

In the real brain, it is not certain which factor among various parameters such as the activity rate  $\varepsilon_\mu$ , the cooperation range  $\sigma_\mu$  and the inhibitory strength  $k_\mu$ , is a major contributor to the anisotropy between OP and OD columns. We can obtain some insights on this by comparing the typical spacings  $\Lambda_{OP}$  and  $\Lambda_{OD}$  measured in animal experiments. Various models predict that the typical spacing  $\Lambda_\mu$  increases in proportion to the cooperation range  $\sigma_\mu$  ( $\Lambda_\mu \propto \sigma_\mu$ ) and decreases for stronger inhibitory strength  $k_\mu$  [5, 18, 19]. If OP and OD columns are different only in the activity rate  $\varepsilon_\mu$ , the typical spacings are the same, that is  $\Lambda_{OD} = \Lambda_{OP}$  for all  $\lambda$ . If they differ only in  $k_\mu$ , the typical spacing of OD bands is usually smaller than that of OP slabs when the strong OD segregation occurs ( $\Lambda_{OD} < \Lambda_{OP}$  for  $\lambda > 1$ ). However, if they differ only in  $\sigma_\mu$ , the typical spacing of OD bands is larger than that of OP slabs when strong OD segregation occurs ( $\Lambda_{OD} > \Lambda_{OP}$  for  $\lambda > 1$ ). Among these possibilities, we find that the last case is consistent with the animal data in cats [9, 12, 20, 21, 22], ferrets [11, 23] and macaque monkeys [8]. This leads us to use the cooperation ranges between columns as the major bifurcation parameter for investigating different visual pattern types in animals. Fig. 3 shows the results of simulations using the typical spacings  $\Lambda_{OP}$  and  $\Lambda_{OD}$  measured in animal experiments. For  $\Lambda_{OD} < \Lambda_{OP}$ , more beaded bands in OD columns emerge near the pinwheel centers as in the visual maps in cats (Fig. 3a), whereas for  $\Lambda_{OD} > \Lambda_{OP}$ , parallel bands in OD columns emerge in a whole region as in macaque monkeys (Fig. 3b).

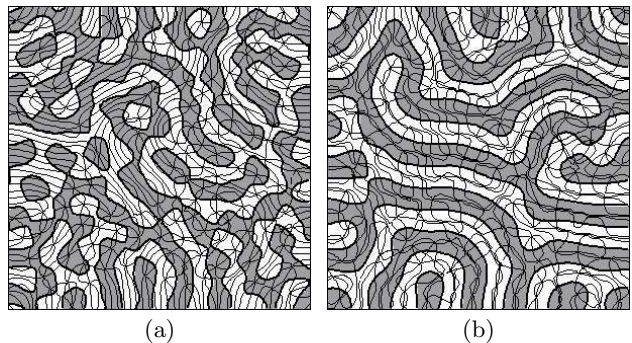


FIG. 3: Simulations of OD and OP maps for (a)  $\Lambda_{OD} < \Lambda_{OP}$  ( $\sigma_{OD}^2 = 6.7$ ,  $\sigma_{OP}^2 = 10.0$ ) and (b)  $\Lambda_{OD} > \Lambda_{OP}$  ( $\sigma_{OD}^2 = 13.8$ ,  $\sigma_{OP}^2 = 10.0$ ). Parameters are  $\varepsilon_{OD} = \varepsilon_{OP}$  and  $k_{OP} = k_{OD} = 0.7$ , so  $\lambda = \sigma_{OD}^2/\sigma_{OP}^2 = \Lambda_{OD}^2/\Lambda_{OP}^2$  ( $100 \times 100$  lattice with a non-periodic boundary condition).

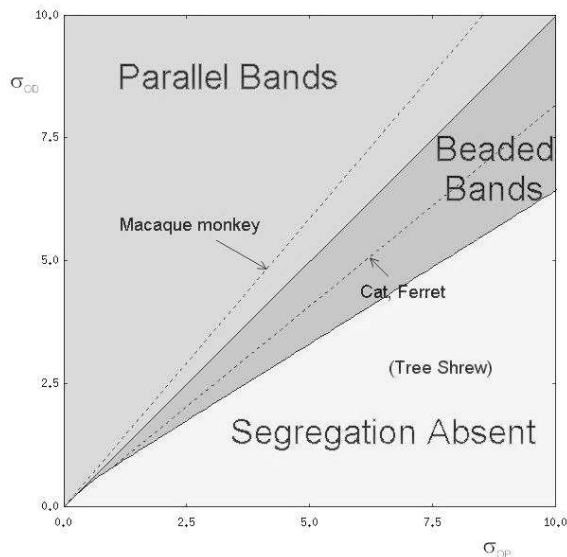


FIG. 4: The phase diagram of OD patterns according to the cooperation ranges,  $\sigma_{OD}$  and  $\sigma_{OP}$ , where dotted lines denote the experimental data for various animals.

The exact calculation of the critical anisotropy  $\lambda_c$ , above which the out-of-plane vortices appear, is also an important problem in magnetism [24]. Unfortunately, any continuum theory fails in calculation of  $\lambda_c$  because of the singularity near the vortex core [25]. The development of out-of-plane components depends on not only the exact form of the interaction function  $D(r)$  but also other factors such as lattice types, vortex distributions, etc. The boundary between the “OD segregation absent” and “Beaded bands” regions cannot be distinguished sharply in both experiments and simulations because the development of OD components is weak near this boundary. The analytic and simulational methods in the CTDAHM can be extended to calculate the critical anisotropy precisely for various cases [26]. We find that the stability boundary of the out-of-plane vortex takes the form  $\sigma_{OD} \simeq \alpha\sigma_{OP} + \beta$ . Since the computed value of  $\beta$  is small, the region for the beaded band pattern can be described by  $\alpha < \sigma_{OD}/\sigma_{OP} < 1$ , where  $\alpha \sim 0.6$  for  $\lambda = \sigma_{OD}^2/\sigma_{OP}^2$ . This agrees well with the experimental data, where  $\Lambda_{OD}/\Lambda_{OP} \sim 0.82$  for cats and ferrets. Fig. 4 shows the phase diagram of different OD pattern formations in the parameter of cooperation ranges,  $\sigma_{OP}$  and  $\sigma_{OD}$ . The experimentally derived curves for macaque monkeys, cats, and ferrets lie well within regions of our predictions.

In this Letter, we showed the influence of the correlation between OP and OD columns on the overall visual map formation, and explained the observed experimental data successfully. Moreover, we also showed that the typical characteristics of emergent cortical maps can be described well by the solutions from the general field theory

with minimal constraints. Our study of the visual map formation suggests another possibility in modeling physical neuronal dynamics with physical models. In spite of the complex circuitry and nonlinear dynamics in neural systems, the neural behavior at high levels may obey simple and general rules, which can be related to the noble theory of statistical physics. We expect to find more applications of physics-based methodology in interpreting diverse neural phenomena and constructing noble computational architecture.

This work was supported by the Ministry of Science and Technology and the Ministry of Education.

\* Electronic address: mwcho@postech.edu

† Electronic address: swan@postech.edu

- [1] E. Erwin, K. Obermayer, and K. Schulten, *Neural comput.* **7**, 425 (1995).
- [2] N. V. Swindale, *Network: Comput. Neural Syst.* **7**, 161 (1996).
- [3] S. Tanaka, in *Theory of self-organization of cortical maps*, edited by D. S. Touretzky (San Mateo, CA: Morgan Kaufmann, 1989), pp. 451–458.
- [4] *Simple spin models for the development of ocular dominance columns and iso-orientation patches*, vol. 3 (1991).
- [5] M. W. Cho and S. Kim, *Phys. Rev. Lett.* **92**, 18101 (2004).
- [6] M. W. Cho and S. Kim (2004), arXiv:q-bio.NC/0405027.
- [7] S. LeVay, D. H. Connolly, J. Houde, and D. C. V. Essen, *J. Neurosci.* **5**, 486 (1985).
- [8] K. Obermayer and G. G. Blasdel, *J. Neurosci.* **13**, 4114 (1993).
- [9] S. Löwel and W. Singer, *Exp. Brain Res.* **68**, 661 (1987).
- [10] P. A. Anderson, J. Olavarria, and R. C. V. Sluyters, *J. Neurosci.* **8**, 2183 (1988).
- [11] J. C. Crowley and L. C. Katz, *Nature Neurosci.* **2**, 1125 (1999).
- [12] S. Löwel, B. Freeman, and W. Singer, *J. Comp. Neurol.* **255**, 401 (1987).
- [13] W. H. Bosking, Y. Zhang, B. R. Schofield, and D. Fitzpatrick, *J. Neurosci.* **17**, 2112 (1997).
- [14] S. Grossberg and S. J. Olson, *Neural Networks* **7**, 883 (1994).
- [15] S. Takeno and S. Homma, *Prog. Theor. Phys.* **64**, 1193 (1980).
- [16] M. E. Gouvêa, G. M. Wysin, A. R. Bishop, and F. G. Mertens, *Phys. Rev. B* **39**, 11840 (1989).
- [17] F. Wolf and T. Geisel, *Nature* **395**, 73 (1998).
- [18] K. Obermayer, G. G. Blasdel, and K. Schulten, *Phys. Rev. A* **45**, 7568 (1992).
- [19] F. Wolf, K. Pawelzik, O. Scherf, T. Geisel, and S. Löwel, *J. Physiol* **94**, 524 (2000).
- [20] S. Löwel, *J. Neurosci.* **14**, 7451 (1994).
- [21] K. Albus, *Exp. Brain Res.* **24**, 181 (1979).
- [22] Y.-C. Diao, J. Jia., N. V. Swindale, and M. S. Cynader, *Exp. Brain Res.* **79**, 271 (1990).
- [23] S. C. Rao, L. J. Toth, and M. Sur, *J. Comp. Neurol.* **387**, 358 (1997).
- [24] J. E. R. Costa and B. V. Costa, *Phy. Rev. B* **54**, 994 (1996).

- [25] W. M. Wysin, *Phy. Rev. B* **49**, 8780 (1994).
- [26] M. W. Cho and S. Kim, *Phy. Rev. B* **70**, 24405 (2004).